 doi:10.20944/preprints202101.0276.v1

Article

Polarization anisotropies in strain-free, asymmetric and symmetric quantum dots grown by droplet epitaxy

Marco Abbarchi [1,*,†,‡], Takaaki Mano [2], Takashi Kuroda [2,‡] and Kazuaki Sakoda [2,‡]

[1] Aix Marseille Univ, Université de Toulon, CNRS, IM2NP Marseille, France
[2] Research Center for Functional Materials, National Institute for Materials Science, 1-1 Namiki, Tsukuba, Ibaraki 305-0044, Japan; MANO.Takaaki@nims.go.jp (T.M.); KURODA.Takashi@nims.go.jp (T.K.); SAKODA.Kazuaki@nims.go.jp (K.S.)
* Correspondence: marco.abbarchi@im2np.fr

Abstract: We provide an extensive and systematic investigation of exciton dynamics in droplet epitaxial quantum dots comparing the cases of (311)A, (001) and (111)A surfaces. In spite of a similar s-shell exciton structure common to the three cases, the absence of a wetting layer for (311)A and (111)A samples leads to a larger carrier confinement with respect to (001), where a wetting layer is present. Moreover, this leads to a more pronounced dependence of the binding energies of s-shell excitons on the quantum dot size and to a strong anti-binding character of the positive charged exciton for smaller quantum dots. In-plane geometrical anisotropies of (311)A and (001) quantum dots lead to a large electron-hole fine interaction (fine structure splitting, FSS$\sim$100 μeV) whereas for the three-fold symmetric (111)A counterpart this figure of merit is reduced of about one order of magnitude. In all these cases we do not observe any size dependence of the fine interactions. Heavy-hole/light-hole mixing is present in all the studied cases leading to a broad spread of linear polarization anisotropy (from 0 up to about 50%) irrespective of surface orientation (symmetry of the confinement), fine interactions and nanostructure size. These results are important for the further development of ideal single and entangled photon sources based on semiconductor quantum dots.

Keywords: III-V Quantum dots, Droplet Epitaxy, exciton dynamics

1. Introduction

Droplet epitaxy [1–3] and droplet etching [4–6] (DE) are alternative growth protocols to Stranski-Krastanov for the fabrication of strain-free III-V-based semiconductor quantum dots (QDs). This emerging class of nanostructures has been efficiently exploited for the fabrication of classical optoelectronic devices such as photodetectors [7] lasers [8–12] and quantum emitters [6,13–25] demonstrating the relevance of this approach for realistic applications.

An appealing possibility offered by DE is the growth of nanostructures on different substrate orientation: in addition to the conventional (001), QDs can be grown on the three-fold symmetric (111)A surface [18,19,26–35] (e.g. for the fabrication of sources of entangled photons) and on the highly anisotropic (311)A surface [10,36–44] (e.g. to obtain large QDs density for laser emission). These substrate orientations affect the QDs properties and in turn, their photophysics by modifying the confining potential (e.g. its symmetry) for electrons and holes and are thus a key tool for engineering the exciton dynamics and the corresponding optical properties.

Here we provide a systematic comparison of exciton dynamics of strain-free DE quantum dots grown on (311)A, (001), and (111)A oriented substrates studied by photoluminescence (PL)

Preprints (www.preprints.org) | NOT PEER-REVIEWED | Posted: 14 January 2021 doi:10.20944/preprints202101.0276.v1

spectroscopy of individual QDs. We show that the presence or absence of a wetting layer underneath the QDs modifies the confinement regime, providing a different evolution of the Coulomb interactions between electrons and holes. The presence of asymmetries in the excitonic confining potential lifts the degeneracy of the neutral exciton state, leading to the presence of a large fine structure splitting (FSS) for (311)A and (001) QDs whereas this figure of merit is abruptly reduced for (111)A QDs. In all the samples, irrespective of surface orientation, the trend of the FSS does not show any significant size dependence. Similarly, the linear polarization anisotropy (the fingerprint of mixing between heavy-hole/light-hole states, *hh/lh*) is randomly distributed and does not show any dependence on size nor geometrical asymmetry.

2. Materials and Methods

2.1. Sample fabrication

All the samples were grown on semi-insulating GaAs substrates by conventional solid-source molecular-beam epitaxy system (MBE32 by Riber) with these recipies:

Sample (311)A [44]:

-2 μm-thick $Al_{0.55}Ga_{0.45}As$ layer grown at 500°C
-136 nm-thick $Al_{0.26}Ga_{0.74}As$ core-layer grown at 610 °C
-at the center of the core-layer GaAs QDs were formed by droplet epitaxy. Nominally 1.5 monolayers of Ga grown at a growth speed of about 0.1 monolayers per second, were supplied in absence of As_4 flux at 275 °C for the droplets formation
-The droplets were crystallized into GaAs QDs by supplying a flux of As_4 (2×10^{-6} Torr beam equivalent pressure) at 200 °C
-the temperature was risen up to 400 °C for 10 minutes under As_4 to improve the crystal quality of the QDs
-the QDs were capped with a 30 nm-thick $Al_{0.26}Ga_{0.74}As$ at 400 °C
-the rest of the $Al_{0.26}Ga_{0.74}As$ (38 nm) layer was grown at 625 °C
-once the entire growth sequence was completed, a rapid thermal annealing process was performed at 785 °C for 4 minutes in an As_4 atmosphere to improve the optical quality[9,45].

Sample (001) [46]:

-a thick $Al_{0.3}Ga_{0.7}As$ barrier layer was grown at 580°C
-the substrate temperature was lowered at 350°C together with reduction of the As pressure
-1.5 monolayers of Ga were supplied for Ga droplet formation
-the As_4 flux was increased to 2×10^{-4} Torr (beam equivalent pressure) to crystallize Ga droplets into GaAs QDs at 200°C
-QDs were annealed *in situ* at 400°C for 10 minutes under As_4 flux irradiation
-40 nm thick $Al_{0.3}Ga_{0.7}As$ capping layer was grown by standard MBE at 400°C
-growth of a 20 nm thick $Al_{0.3}Ga_{0.7}As$ layer at 580°C -growth of 10 nm thick GaAs capping by standard MBE at at 580°C. -finally, the sample was processed with post-growth annealing [9,45].

Sample (111):

- a thick $Al_{0.3}Ga_{0.7}As$ barrier layer was grown at 500°C
-the substrate temperature was lowered 400°C together with reduction of the As pressure
-0.05 monolayers of Ga were supplied for Ga droplet formation
-the As_4 flux was set to 2×10^{-6} Torr beam equivalent pressure to crystallize Ga droplets into GaAs QDs at 200°C
-QDs were annealed *in situ* at 500° for 10 minutes under As_4 flux irradiation
-50 nm thick $Al_{0.3}Ga_{0.7}As$ capping layer was grown by standard MBE at 500°C
-10 nm thick GaAs at were grown at 500°C -finally the sample was annealed at 600°C under As_4 flux to improve the optical quality [9,45].

Preprints (www.preprints.org) | NOT PEER-REVIEWED | Posted: 14 January 2021 doi:10.20944/preprints202101.0276.v1

QDs morphology was studied on samples left uncapped. We used an atomic force microscope (AFM, SPA400 by Hitachi High-Tech) in non-contact mode and an *in situ* STM microscope (only for the (111)A sample).

2.2. Optical spectroscopy

For photoluminescence spectroscopy measurements (PL) of individual nanostructures, the samples were kept in a liquid-helium cryostat at about 10 K. The PL signal was collected with a custom-made confocal-spectroscopic setup having a diffraction-limited lateral resolution of about 1 μm. Excitation was performed above barrier energy with a CW laser at 532 nm (about 2.3 eV). The PL signal was analysed with a spectrometer and detected by a Si-based CCD camera, allowing for a spectral resolution better than 25 μeV in full width at half maximum (FWHM). The PL signal was discriminated in polarization by using a linear polariser and a half wave plate.

3. Results and discussion

3.1. Morphology of droplet epitaxial quantum dots on (311)A, (001) and (111)A surfaces

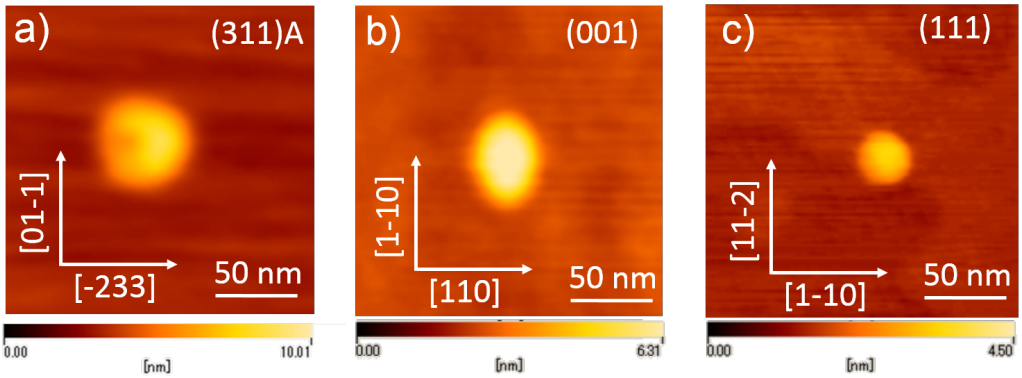

Figure 1. (**a**) AFM image of a QD grown on the (311)A surface. (**b**) AFM image of a QD on the (001) surface. (**c**) AFM image of a QD on the (111)A surface.

We first provide a description of the main morphological features of QDs grown on differently oriented surfaces. The three samples ((311)A, (001) and (111)A) where characterised by AFM (Figure 1). For the sake of thoroughness, we mention that the QDs that are selected for AFM are likely much larger than those characterized in PL [47,48]. We also mention that the effect of capping after QDs formation should not affect the final shape of the nanostructures [9] .

QDs grown on the (311)A surface have a rather complex morphology (Figure 1 a) that is ascribed to the low AS_4 pressure and to the strong asymmetry of the underlying substrate [10,36,37,39–43]. Owing to the non-equivalent adatom diffusion along the oppositely oriented directions [-233] and [2-3-3], the crystallization process from metallic droples into GaAs QDs is occurring at different rates on one side ([-233]). Instead of forming rings with a central hole as for the conventional (001) case [9,14,44,49–54], they feature a U-shape with two protrusions along the [-233] direction, that is specific of this surface orientation.

QDs grown by DE on the conventional (001) surface have been extensively studied in the past years [46,55–58] (Figure 1 b). The sample studied here was grown with an improved DE method, including a high temperature annealing step at 400°C [46]. This step is crucial to improve the crystal quality (e.g. to reduce the formation of As precipitates in the top barrier [59]) and in turn the PL properties of exciton recombination. A side effect of this annealing step is an increase of the elongation of QDs: typically this kind of sample features a more pronounced asymmetry along the [1-10] direction

Preprints (www.preprints.org) | NOT PEER-REVIEWED | Posted: 14 January 2021 doi:10.20944/preprints202101.0276.v1

(that is the direction of maximal surface diffusion on this surface orientation) with respect to samples with lower growth temperature [55] and lesser optical quality.

QDs grown on the (111)A surface are typically more symmetric with respect to the previous two cases, thanks to the three-fold symmetry of the underlying substrate orientation [18,19,26–35]. Triangular and hexagonal structures can be formed, depending on the growth conditions [26,27].

3.2. s-shell excitons in droplet epitaxial quantum dots

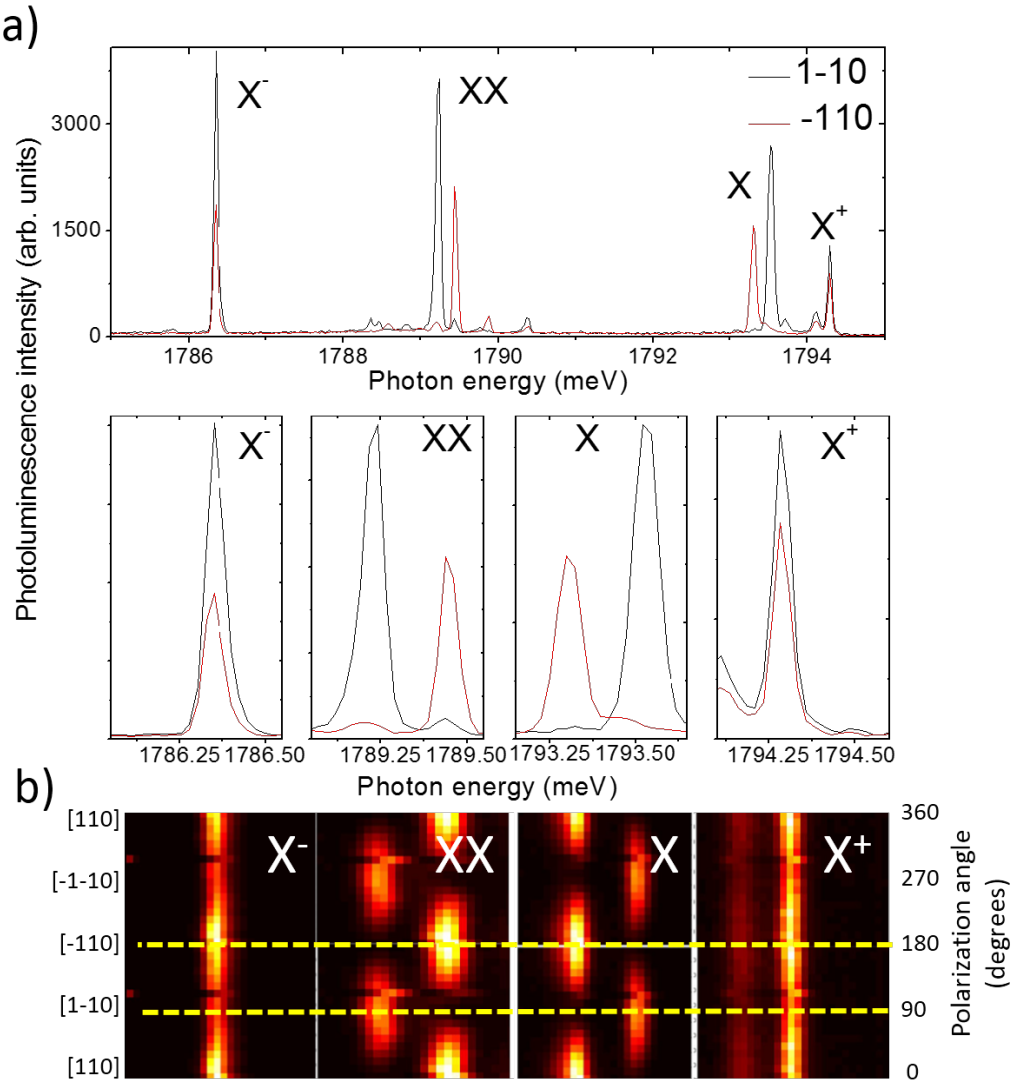

Figure 2. (**a**) Top panel: photoluminescence (PL) spectrum of a QD grown on the (001) surface. The main excitonic recombination lines from the s-shell are highlighted. Red and black lines represent the orthogonally, linearly polarized components of the PL respectively oriented along the crystallographic axes [-110] and [1-10]. Bottom Panels: from the left to the right panel are shown blow-up of each individual line in the spectrum, respectively X^{-}, XX, X and X^{+} for both linearly polarized components. (**b**) From the left to the right panel are represented the intensity change (represented as a color-scale) of the s-shell excitons as a function of the detected polarization angle. The horizontal dashed lines highlight the polarization represented in **a**.

PL spectroscopy is systematically used to investigate the electronic properties of QDs. In the following sections we address the main PL components of (311)A, (001) and (111)A QDs. As an

Preprints (www.preprints.org) | NOT PEER-REVIEWED | Posted: 14 January 2021 doi:10.20944/preprints202101.0276.v1

example, we show the conventional case of (001) QDs (Figure 1). The two others, (311)A and (111)A, are characterised by the same structure and are not explicitly reported.

As for the conventional case of Stranski Krastanov growth, s-shell excitons in DE QDs are the neutral exciton and biexciton (respectively X and XX), positively and negatively charged excitons (respectively X^+ and X^-) (Figure 2). The assessment of each spectral component of the s-shell excitons has been largely discussed in previous works [19,26,38,44,55,60–63] and is not repeated here.

From this kind of spectra we can recover several information concerning the exciton dynamics: i) the binding energy of XX, X^+ and X^- measured as energy distance between an excitonic PL and the corresponding X line (Figure 2 a top panel), ii) the fine Coulomb interaction between carriers spins measured as energy splitting of the two linearly polarized components of X and XX PL lines (Figure 2 a, bottom panel) and iii) the mixing between *hh* and *lh* states, measured from the polar diagram of PL intensity as a function of the detected polarization angle (as in Figure 2 b).

These three important features of the photophysics of excitons in QDs will be comparatively addressed for the (001), (111)A and (311)A cases. In the specific case under study and unlike for the Stranski Krastanov counterpart, these figures of merits are not influenced by strain and related piezoelectric fields, thus simplifying the overall picture and allowing to directly link the observation to the geometrical parameters of the nanostructures (e.g. asymmetry, orientation with respect to the crystallographic axes) and to heavy-hole, light-hole mixing.

3.3. Binding energy of s-shell excitons

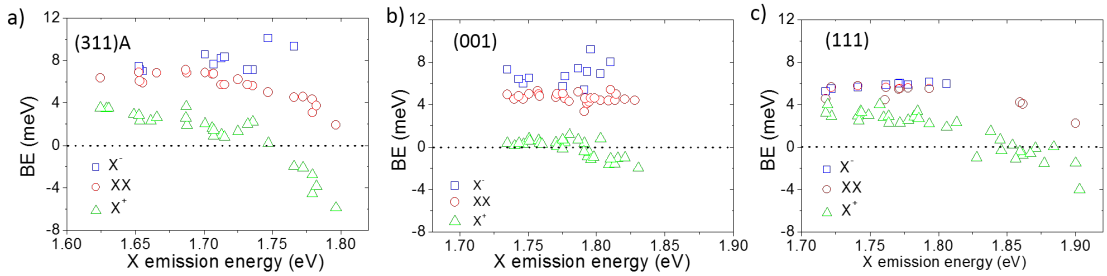

Figure 3. (**a**) Binding energy of XX, X^+ and X^- for (311)A QDs as a function of X emission energy, re-plotted from reference [38]. (**b**) Same as **a** for (001) QDs, re-plotted from reference [38]. (**c**) Same as **a** for (111)A QDs.

The emission energy of all the PL lines with respect to the corresponding X line can be used to directly assess the binding energy (BE): the energy difference between X and the other lines is a measure of the Coulomb interactions within an excitonic complex [38,64–66]. We performed this analysis for the three surfaces on a large number of QDs spanning an interval of about 200 meV of X emission energy (Figure. 3). For the sake of thoroughness, we mention that the interval of X emission energy is slightly lower for the (311)A case owing to a lower Al content in the barrier material in this sample with respect to the others.

The overall picture common to all the samples is described as follows [38]: XX and X^- have a binding character whereas X^+ changes from binding to anti-binding when increasing X emission energy (that is reducing QD size). More precisely, the BE of X^- shows a weak increase (although its behavior is quite scattered for (311)A and (001) cases and this exciton complex is not observed in smaller QDs) whereas that of XX, X^+ decreases. The BE of XX and X^+ changes smoothly for the (001) case (changes are in the 4 meV range, Figure. 3 b), whereas are more abrupt for the (311)A and (111)A cases (5-10 meV, Figure. 3 a and c).

This complex behavior is determined by the combination of attractive and repulsive Coulomb forces between the carriers composing the different excitonic species. Owing to the presence of several particles composing the excitons in the s-shell, the overall picture can be qualitatively understood by considering the mean-field corrections and correlation effects necessary to account for the many-body

Preprints (www.preprints.org) | NOT PEER-REVIEWED | Posted: 14 January 2021 doi:10.20944/preprints202101.0276.v1

character of the problem. The larger *hh* mass with respect to the *e* one in GaAs results in a larger localization within the QD and a correspondingly larger carrier density for the holes [67]. This difference is responsible for a larger repulsive interaction in X^+ that leads to a decreasing BE and an anti-binding character for smaller nanostructures. For the same reason, the interaction between an *e* and a *hh* results in a mean field that is attractive for an extra-electron, leading to a binding character of X^- and in increase in its BE in smaller QDs, as shown by the experimental data (Figure 3).

A more refined theoretical framework based on a quantum Monte-Carlo approach for strain-free QDs [68–70], was developed in reference [38] to account for the difference between a truly 3D confinement with respect to a weaker lateral confinement. This model explains the differences between the steep changes of the BE for excitons in (311)A and (111)A cases with respect to the (001) case. In the former scenario the lack of wetting layer in (311)A and (111)A, results in a stronger carrier confinement and thus in an overall picture that can be captured by a spherical potential (strong confinement in all the directions). In the case of (001) instead, the presence of a wetting layer results in a weaker lateral confinement (strong confinement only along the vertical growth direction) and a behavior that can be described by a shallow disk. Thus, the presented results confirm that also in (111)A QDs the strong confinement regime holds as for the (311)A case [38].

3.4. Electron-hole spin interactions, fine structure splitting

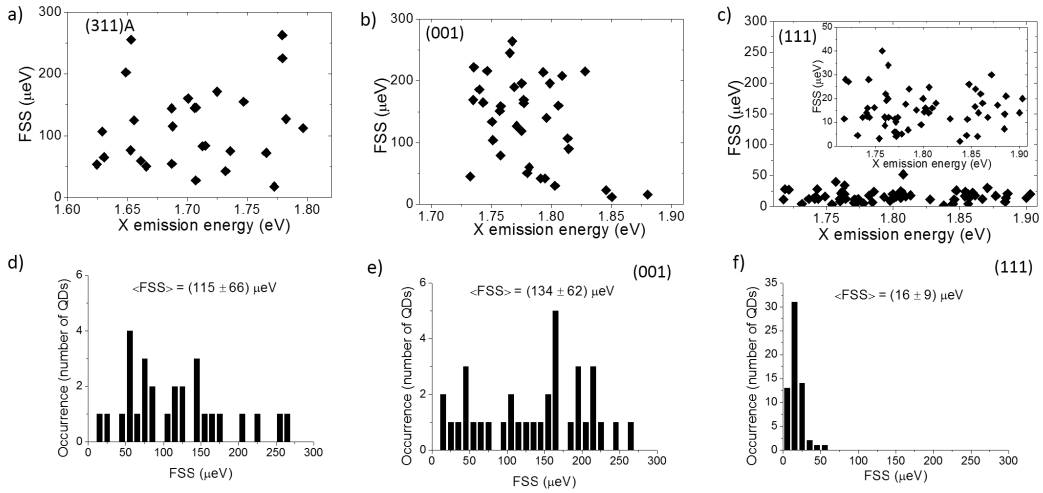

Figure 4. (**a**) Fine structure splitting (FSS) as a function of the X emission energy for (311)A QDs. (**b**) Fine structure splitting as a function of the X emission energy for (001) QDs. (**c**) Fine structure splitting as a function of the X emission energy for (111)A QDs. The inset show the same data rescaled for clarity. **d**, **e**, and **f** are statistical distribution of the FSS respectively corresponding to graph **a**, **b**, **c**.

The study of the linear polarization dependence of the s-shell excitons emission allows to measure the polarization splitting of each PL line (Figure 2 b)) [71]. Generally speaking, X and XX show a mirror symmetric polarization splitting, being the fingerprint of electron-hole fine interactions [55,72–74]. X^+ does not show any energy splitting, being the fine interactions in the initial state (two holes in valence band with opposite spin, interacting with an electron in conduction band) and in the final state (one hole in valence band) of the recombination paths zero. Similar consideration holds for the negative charged exciton counterpart X^-. Beyond fundamental physics, this feature is extremely relevant for the implementation of entangled photon emission springing from XX-X cascaded photons pairs [23–25,75], provided that the fine structure splitting (FSS) is negligible and the *which-path-information* erased.

Here we studied the FSS for the three samples exploring the cases of large anisotropy (311)A, lower anisotropy (001) and vanishing anisotropy (111)A (Figure 4). In all the cases no size dependence is observed with fluctuations that are in the 300 μeV range for (311)A and (001) cases and about one order of magnitude lower for the (111)A counterpart (Figure 4 a, b and c). The statistical analysis

Preprints (www.preprints.org) | NOT PEER-REVIEWED | Posted: 14 January 2021 doi:10.20944/preprints202101.0276.v1

shows an average FSS of 155 $\pm$ 66 μeV for (311)A, 134 $\pm$ 62 μeV for (001) and 16 $\pm$ 9 μeV for (111)A, the error being the standard deviation of the distribution (Figure 4 d, e and f).

These results confirm that the anisotropic surface diffusion of GaAs adatoms during QDs growth atop AlGaAs results in large shape anisotropies that break the in-plane symmetry of the QDs. In spite of the lack of piezoelectricity in these strain-free nanostructures, the geometric anisotropy promotes the fine interaction between electron and hole spins in the X state, lifts its degeneracy and leads to energy distinguishable recombination paths from the XX to the X state limiting the possibility to obtain entangled photon pairs. Thus, although the FSS can be reduced *a posteriori* via strain tuning [58] extending the use of anisotropic surfaces for the fabrication of entangled photon sources, the use of three-fold symmetric (111)A surfaces is clearly favorable for this task [19,20,22].

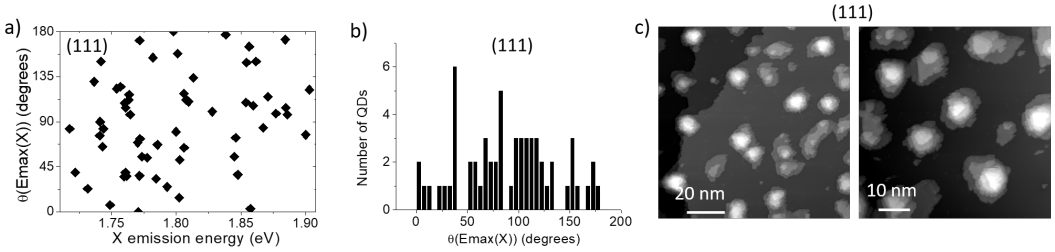

Figure 5. a) Polarization angle $\theta(E_{max}(X))$ corresponding to the high energy split component of the X doublet for (111)A QDs (as obtained from the polarization analysis shown in Figure 2 b) as a function of the corresponding X emission energy. An angle of 0 degrees correspond to the in plane [1-12] direction. b) Statistical distribution of $\theta(E_{max}(X))$. c) High-resolution *in vacuo* STM micrographs of an ensemble of GaAs QDs sitting on (111)A-oriented AlGaAs.

From the same investigation it is possible to determine the directions of the polarization axes of the split PL components with respect to the crystallographic axes (Figure 2 b, and Figure 5). As previously reported for the (001) case [76], for high quality DE nanostructures grown at larger temperature, the morphology of the QDs shows a marked elongation along the [1-10] in-plane direction (that is at the basis of the FSS measured in these kind of samples) and the two orthogonally polarized PL components are mostly aligned along these axes (as highlighted in Figure 2 b by the horizontal, dashed, yellow lines). This observation holds for the large majority of the QDs grown on the (311)A and (001) surfaces (not shown) but it is not verified in the (111)A case (Figure 5). By reporting the angle of the high energy split component ($\theta(E_{max}(X))$) for the (111)A case as a function of the corresponding X emission energy and the corresponding statistical distribution (respectively Figure 5 a and b), we observe a completely random behavior. *In vacuo* STM, high resolution micrographs from a (111)A sample (grown in similar conditions of those studied in PL), reveal that the QDs are composed by piles of terraces, forming a truncated pyramid and do not feature any preferential elongation in a specific direction (Figure5 c). These observations justify that there is no dependence of the FSS with QDs size nor a preferential axis for the two PL split components.

Preprints (www.preprints.org) | NOT PEER-REVIEWED | Posted: 14 January 2021 doi:10.20944/preprints202101.0276.v1

3.5. Heavy-hole/light-hole mixing

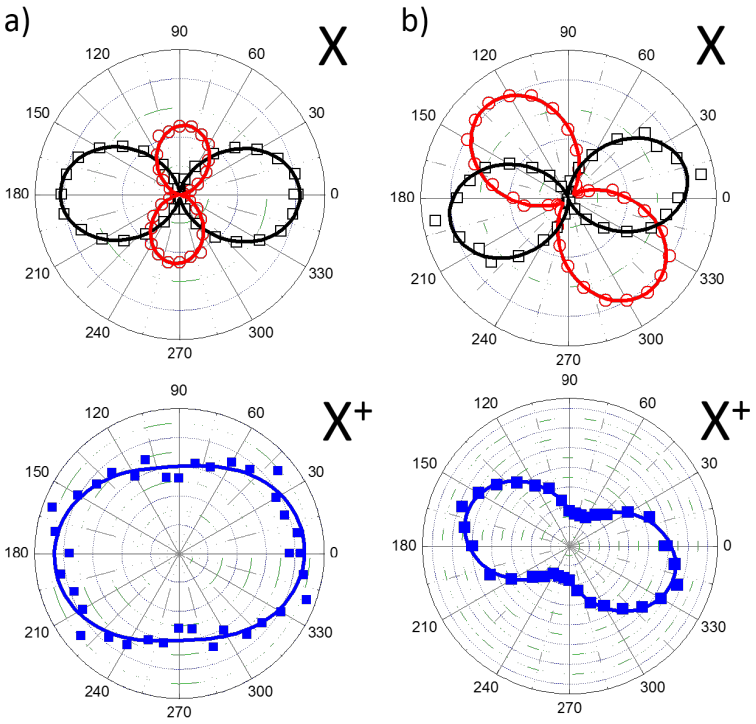

Figure 6. **a** Polar diagram of X PL intensity (top panel) and X^+ PL intensity as obtained from the polarization dependence shown in Figure 2**b** for a QD grown on the (001) surface and having a geometrical asymmetry oriented along the main crystallographic axes. **b** Same as **a** but for a QD with an elongation tilted with respect to the main crystallographic axes.

Another feature emerging from the characterization of the PL spectra of single QDs when detected as a function of the polarization angle, is a different intensity of the two split components of X and XX (Figure 2 b), Figure 6). This is the signature of a relevant mixing between *hh* and *lh* states leading to non-pure selection rules for electron and hole recombination [77–83,83,84]. In III-V QDs, the bottom of the conduction band can be described, to a first approximation, with an isotropic and parabolic dispersion. Valence bands instead, are characterised by the presence of *hh* and *lh* states that are tens of meV far apart. Their bands dispersion feature a large anisotropy and different curvatures (different effective masses). In Stranski Krastanov QDs the presence of piezoelectricity results in a large *hh-lh* mixing [78,79,81–83] and finally, uneven PL intensity for the recombination paths of electrons and holes, owing to different selection rules.

The same features were firstly found in (001), strain-free DE QDs with shape asymmetries [77,80]. The presence of an elongation along a crystallographic axis results in uneven PL intensity of the two orthogonally polarized components of the X line. This feature can be conveniently represented in a polar plot of the high- and low-energy components of the X split doublet (Figure6 a, top panel). The same effect can be observed in all the s-shell excitons (Figure2 b), allowing to focus, for instance, on the X^+ line only (Figure6 a and b, bottom panels). This possibility is particularly convenient for QDs having a very small FSS, as those grown on the (111)A substrate, where the two PL lines of the X split doublet cannot be easily resolved, owing to the limited spectral resolution of the spectrometer in use and comparably large FSS and line broadening.

Another important feature to take into account to explain the polarization anisotropy and the effect of *hh-lh* mixing is the orientation of the QD in-plane elongation with respect to the crystallographic axes. An orientation of the polarization axes parallel to the in-plane, main crystallography directions,

Preprints (www.preprints.org) | NOT PEER-REVIEWED | Posted: 14 January 2021 doi:10.20944/preprints202101.0276.v1

is the signature of a geometrical elongation of the QD shape along these directions (as in Figure6 a) [77,79,80]. A different orientation of the geometrical elongation results in a rotation of the polar diagram with respect to the main crystallographic axes and in non-orthogonal relative orientation between the two PL split lines (as in Figure6 b) [77,79,80]. Note that the direction defined by the polarization diagram is not necessarily aligned to the in-plane elongation axis of the QD.

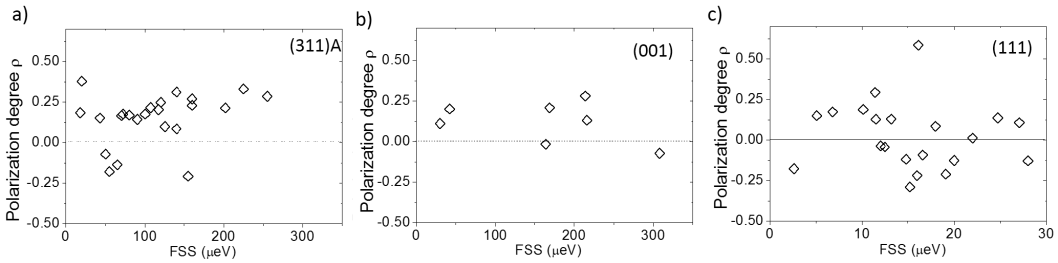

Figure 7. (**a**) Polarization degree of the X PL line as a function of the corresponding FSS for QDs grown on the (311)A surface. (**b**) Same as **a** for (001) QDs. (**c**) Same as **a** for (111)A QDs.

These scenarios are observed in all the investigated samples (not shown). For (311)A case, more than half of the QDs show an alignment along [01-1] or [-233] directions, whereas about 40% are randomly oriented. Thus, in spite of the large anisotropy of this surface, the complex shape of the QDs can induce a disordered polarization orientation. This may be linked to small differences in the two protrusions of the QD along the [-233] direction (Figure 1 a). For QDs grown on (001) surface we observe that the large majority shows an almost perfect alignment (within a few degrees) of the polarization axes along the [1-10] main crystallographic direction, with very few exceptions (as that one shown in Figure6 b), accounting for their preferential geometrical elongation [77,79,80] in these directions (Figure1 b). Finally, for (111)A QDs, the lack of a preferential elongation of the QDs results in a completely randomised orientation of the polarization directions (see for instance Figure5 a and b).

Thus, provided the larger symmetry of the (111)A QDs with respect to the others presented here, the corresponding FSS is indeed smaller and the orientation of the polarization axes (and underling geometrical anisotropy) completely random. However, in spite of this larger symmetry, the polarization anisotropy ($\rho = (I_{max} - I_{min})/(I_{max} + I_{min})$) fluctuates in the same range for all the threes cases. By plotting ρ as a function of the corresponding FSS (Figure7) or X emission energy (not shown), we observe no dependence of the *hh-lh* mixing on shape anisotropy (FSS) nor size (X emission energy) and no reduction for the (111)A case with respect to the others.

4. Conclusions

In conclusion we showed that DE is a versatile technique for the growth of high quality III-V QDs on differently oriented substrate. The s-shell exciton dynamics is strongly influenced by the presence or absence of a wetting layer. A strong lateral confinement is found for (311)A and (111)A QDs in contrast with the (001) case where the carrier confinement is weaker. This results in a marked difference in the Coulomb interaction between electrons and holes composing the s-shell excitons. The presence of geometrical asymmetries in the QDs shape leads to a rather large fine interaction between electrons and holes spins for the anisotropic surfaces (311)A and (001) whereas for the three-fold symmetric (111)A case this figure of merit is in the 10μeV range. However, in spite of the increased symmetry of the confining potential, a relevant polarization anisotropy is found also for this latter case, pointing to a relevant mixing between heavy- and light-hole states in the valence band.

Funding:

Acknowledgments:

Conflicts of Interest: The authors declare no conflict of interest.

 doi:10.20944/preprints202101.0276.v1

Abbreviations

The following abbreviations are used in this manuscript:

PL	photoluminescence
QD	quantum dot
FSS	fine structure splitting
X	neutral exciton
X^+	positive charged exciton
XX	neutral biexciton
X^-	negative charged exciton
FWHM	full width at half maximum
hh	heavy hole
lh	light hole
e	electron

1. Mantovani, V.; Sanguinetti, S.; Guzzi, M.; Grilli, E.; Gurioli, M.; Watanabe, K.; Koguchi, N. Low density GaAs/ AlGaAs quantum dots grown by modified droplet epitaxy. *Journal of applied physics* **2004**, *96*, 4416–4420.
2. Wu, J.; Wang, Z.M. Droplet epitaxy for advanced optoelectronic materials and devices. *Journal of Physics D: Applied Physics* **2014**, *47*, 173001.
3. Gurioli, M.; Wang, Z.; Rastelli, A.; Kuroda, T.; Sanguinetti, S. Droplet epitaxy of semiconductor nanostructures for quantum photonic devices. *Nature materials* **2019**, p. 1.
4. Atkinson, P.; Zallo, E.; Schmidt, O. Independent wavelength and density control of uniform GaAs/AlGaAs quantum dots grown by infilling self-assembled nanoholes. *Journal of Applied Physics* **2012**, *112*, 054303.
5. Huo, Y.; Rastelli, A.; Schmidt, O. Ultra-small excitonic fine structure splitting in highly symmetric quantum dots on GaAs (001) substrate. *Applied Physics Letters* **2013**, *102*, 152105.
6. Huber, D.; Reindl, M.; Huo, Y.; Huang, H.; Wildmann, J.S.; Schmidt, O.G.; Rastelli, A.; Trotta, R. Highly indistinguishable and strongly entangled photons from symmetric GaAs quantum dots. *Nature communications* **2017**, *8*, 1–7.
7. Vichi, S.; Bietti, S.; Khalili, A.; Costanzo, M.; Cappelluti, F.; Esposito, L.; Somaschini, C.; Fedorov, A.; Tsukamoto, S.; Rauter, P.; others. Droplet epitaxy quantum dot based infrared photodetectors. *Nanotechnology* **2020**, *31*, 245203.
8. Mano, T.; Kuroda, T.; Yamagiwa, M.; Kido, G.; Sakoda, K.; Koguchi, N. Lasing in Ga As/ Al Ga As self-assembled quantum dots. *Applied physics letters* **2006**, *89*, 183102.
9. Mano, T.; Kuroda, T.; Mitsuishi, K.; Yamagiwa, M.; Guo, X.J.; Furuya, K.; Sakoda, K.; Koguchi, N. Ring-shaped GaAs quantum dot laser grown by droplet epitaxy: effects of post-growth annealing on structural and optical properties. *Journal of crystal growth* **2007**, *301*, 740–743.
10. Mano, T.; Kuroda, T.; Mitsuishi, K.; Nakayama, Y.; Noda, T.; Sakoda, K. Ga As/ Al Ga As quantum dot laser fabricated on GaAs (311) A substrate by droplet epitaxy. *Applied Physics Letters* **2008**, *93*, 203110.
11. Jo, M.; Mano, T.; Sakoda, K. Lasing in ultra-narrow emission from GaAs quantum dots coupled with a two-dimensional layer. *Nanotechnology* **2011**, *22*, 335201.
12. Jo, M.; Mano, T.; Sakoda, K. Electrical Lasing in GaAs Quantum Dots Grown by Droplet Epitaxy. Advances in Optical Materials. Optical Society of America, 2012, pp. ITh5B–6.
13. Kuroda, T.; Abbarchi, M.; Mano, T.; Watanabe, K.; Yamagiwa, M.; Kuroda, K.; Sakoda, K.; Kido, G.; Koguchi, N.; Mastrandrea, C.; others. Photon correlation in GaAs self-assembled quantum dots. *Applied physics express* **2008**, *1*, 042001.
14. Abbarchi, M.; Mastrandrea, C.; Vinattieri, A.; Sanguinetti, S.; Mano, T.; Kuroda, T.; Koguchi, N.; Sakoda, K.; Gurioli, M. Photon antibunching in double quantum ring structures. *Physical Review B* **2009**, *79*, 085308.
15. Abbarchi, M.; Kuroda, T.; Mano, T.; Gurioli, M.; Sakoda, K. Bunched photon statistics of the spectrally diffusive photoluminescence of single self-assembled GaAs quantum dots. *Physical Review B* **2012**, *86*, 115330.

16. Benyoucef, M.; Zuerbig, V.; Reithmaier, J.P.; Kroh, T.; Schell, A.W.; Aichele, T.; Benson, O. Single-photon emission from single InGaAs/GaAs quantum dots grown by droplet epitaxy at high substrate temperature. *Nanoscale research letters* **2012**, *7*, 1–5.
17. Kumano, H.; Nakajima, H.; Kuroda, T.; Mano, T.; Sakoda, K.; Suemune, I. Nonlocal biphoton generation in a Werner state from a single semiconductor quantum dot. *Physical review B* **2015**, *91*, 205437.
18. Kumano, H.; Harada, T.; Suemune, I.; Nakajima, H.; Kuroda, T.; Mano, T.; Sakoda, K.; Odashima, S.; Sasakura, H. Stable and efficient collection of single photons emitted from a semiconductor quantum dot into a single-mode optical fiber. *Applied Physics Express* **2016**, *9*, 032801.
19. Kuroda, T.; Mano, T.; Ha, N.; Nakajima, H.; Kumano, H.; Urbaszek, B.; Jo, M.; Abbarchi, M.; Sakuma, Y.; Sakoda, K.; others. Symmetric quantum dots as efficient sources of highly entangled photons: Violation of Bell's inequality without spectral and temporal filtering. *Physical Review B* **2013**, *88*, 041306.
20. Basso Basset, F.; Bietti, S.; Reindl, M.; Esposito, L.; Fedorov, A.; Huber, D.; Rastelli, A.; Bonera, E.; Trotta, R.; Sanguinetti, S. High-yield fabrication of entangled photon emitters for hybrid quantum networking using high-temperature droplet epitaxy. *Nano letters* **2018**, *18*, 505–512.
21. Ramírez, H.Y.; Chou, Y.L.; Cheng, S.J. Effects of electrostatic environment on the electrically triggered production of entangled photon pairs from droplet epitaxial quantum dots. *Scientific reports* **2019**, *9*, 1–10.
22. Ha, N.; Mano, T.; Kuroda, T.; Sakuma, Y.; Sakoda, K. Current-injection quantum-entangled-pair emitter using droplet epitaxial quantum dots on GaAs (111) A. *Applied Physics Letters* **2019**, *115*, 083106.
23. Basset, F.B.; Rota, M.B.; Schimpf, C.; Tedeschi, D.; Zeuner, K.D.; da Silva, S.C.; Reindl, M.; Zwiller, V.; Jöns, K.D.; Rastelli, A.; others. Entanglement swapping with photons generated on demand by a quantum dot. *Physical Review Letters* **2019**, *123*, 160501.
24. Basset, F.B.; Valeri, M.; Roccia, E.; Muredda, V.; Poderini, D.; Neuwirth, J.; Spagnolo, N.; Rota, M.B.; Carvacho, G.; Sciarrino, F.; others. Quantum key distribution with entangled photons generated on-demand by a quantum dot. *arXiv preprint arXiv:2007.12727* **2020**.
25. Basset, F.B.; Salusti, F.; Schweickert, L.; Rota, M.B.; Tedeschi, D.; da Silva, S.F.C.; Roccia, E.; Zwiller, V.; Jöns, K.D.; Rastelli, A.; others. Quantum Teleportation with Imperfect Quantum Dots. *arXiv preprint arXiv:2006.02733* **2020**.
26. Mano, T.; Abbarchi, M.; Kuroda, T.; McSkimming, B.; Ohtake, A.; Mitsuishi, K.; Sakoda, K. Self-assembly of symmetric GaAs quantum dots on (111) A substrates: Suppression of fine-structure splitting. *Applied physics express* **2010**, *3*, 065203.
27. Jo, M.; Mano, T.; Abbarchi, M.; Kuroda, T.; Sakuma, Y.; Sakoda, K. Self-limiting growth of hexagonal and triangular quantum dots on (111) A. *Crystal growth & design* **2012**, *12*, 1411–1415.
28. Liu, X.; Ha, N.; Nakajima, H.; Mano, T.; Kuroda, T.; Urbaszek, B.; Kumano, H.; Suemune, I.; Sakuma, Y.; Sakoda, K. Vanishing fine-structure splittings in telecommunication-wavelength quantum dots grown on (111) A surfaces by droplet epitaxy. *Physical Review B* **2014**, *90*, 081301.
29. Bouet, L.; Vidal, M.; Mano, T.; Ha, N.; Kuroda, T.; Durnev, M.; Glazov, M.; Ivchenko, E.; Marie, X.; Amand, T.; others. Charge tuning in [111] grown GaAs droplet quantum dots. *Applied Physics Letters* **2014**, *105*, 082111.
30. Ohtake, A.; Ha, N.; Mano, T. Extremely high-and low-density of Ga droplets on GaAs {111} A, B: Surface-polarity dependence. *Crystal Growth & Design* **2015**, *15*, 485–488.
31. Ha, N.; Mano, T.; Wu, Y.N.; Ou, Y.W.; Cheng, S.J.; Sakuma, Y.; Sakoda, K.; Kuroda, T. Wavelength extension beyond 1.5 μm in symmetric InAs quantum dots grown on InP (111) A using droplet epitaxy. *Applied Physics Express* **2016**, *9*, 101201.
32. Mano, T.; Mitsuishi, K.; Ha, N.; Ohtake, A.; Castellano, A.; Sanguinetti, S.; Noda, T.; Sakuma, Y.; Kuroda, T.; Sakoda, K. Growth of metamorphic InGaAs on GaAs (111) a: counteracting lattice mismatch by inserting a thin InAs interlayer. *Crystal Growth & Design* **2016**, *16*, 5412–5417.
33. Trapp, A.; Reuter, D. Formation of self-assembled GaAs quantum dots via droplet epitaxy on misoriented GaAs (111) B substrates. *Journal of Vacuum Science & Technology B, Nanotechnology and Microelectronics: Materials, Processing, Measurement, and Phenomena* **2018**, *36*, 02D106.
34. Ha, N.; Mano, T.; Dubos, S.; Kuroda, T.; Sakuma, Y.; Sakoda, K. Single photon emission from droplet epitaxial quantum dots in the standard telecom window around a wavelength of 1.55 μm. *Applied Physics Express* **2020**, *13*, 025002.

35. Bietti, S.; Basset, F.B.; Tuktamyshev, A.; Bonera, E.; Fedorov, A.; Sanguinetti, S. High–temperature droplet epitaxy of symmetric GaAs/AlGaAs quantum dots. *Scientific Reports* **2020**, *10*, 1–10.
36. Jo, M.; Keizer, J.G.; Mano, T.; Koenraad, P.M.; Sakoda, K. Self-assembly of GaAs quantum wires grown on (311) A substrates by droplet epitaxy. *Applied physics express* **2011**, *4*, 055501.
37. Mano, T.; Kuroda, T.; Mitsuishi, K.; Noda, T.; Sakoda, K. High-density GaAs/AlGaAs quantum dots formed on GaAs (3 1 1) A substrates by droplet epitaxy. *Journal of crystal growth* **2009**, *311*, 1828–1831.
38. Abbarchi, M.; Kuroda, T.; Mano, T.; Sakoda, K.; Mastrandrea, C.A.; Vinattieri, A.; Gurioli, M.; Tsuchiya, T. Energy renormalization of exciton complexes in GaAs quantum dots. *Physical Review B* **2010**, *82*, 201301.
39. Kawazu, T.; Noda, T.; Mano, T.; Jo, M.; Sakaki, H. Effects of antimony flux on morphology and photoluminescence spectra of GaSb quantum dots formed on GaAs by droplet epitaxy. *Journal of Nonlinear Optical Physics & Materials* **2010**, *19*, 819–826.
40. Mano, T.; Noda, T.; Kuroda, T.; Sanguinetti, S.; Sakoda, K. Self-assembled GaAs quantum dots coupled with GaAs wetting layer grown on GaAs (311) A by droplet epitaxy. *physica status solidi c* **2011**, *8*, 257–259.
41. Keizer, J.; Jo, M.; Mano, T.; Noda, T.; Sakoda, K.; Koenraad, P. Structural atomic-scale analysis of GaAs/AlGaAs quantum wires and quantum dots grown by droplet epitaxy on a (311) A substrate. *Applied Physics Letters* **2011**, *98*, 193112.
42. Keizer, J.; Koenraad, P. Atomic-scale analysis of self-assembled quantum dots by cross-sectionalscanning, tunneling microscopy, and atom probe tomography. In *Quantum Dots: Optics, Electron Transport and Future Applications*; Cambridge University Press, 2012; pp. 41–60.
43. Saidi, F.; Bouzaiene, L.; Sfaxi, L.; Maaref, H. Growth conditions effects on optical properties of InAs quantum dots grown by molecular beam epitaxy on GaAs (1 1 3) A substrate. *Journal of luminescence* **2012**, *132*, 289–292.
44. Abbarchi, M.; Mano, T.; Kuroda, T.; Sakoda, K. Exciton Dynamics in Droplet Epitaxial Quantum Dots Grown on (311) A-Oriented Substrates. *Nanomaterials* **2020**, *10*, 1833.
45. Sanguinetti, S.; Mano, T.; Gerosa, A.; Somaschini, C.; Bietti, S.; Koguchi, N.; Grilli, E.; Guzzi, M.; Gurioli, M.; Abbarchi, M. Rapid thermal annealing effects on self-assembled quantum dot and quantum ring structures. *Journal of Applied Physics* **2008**, *104*, 113519.
46. Mano, T.; Abbarchi, M.; Kuroda, T.; Mastrandrea, C.; Vinattieri, A.; Sanguinetti, S.; Sakoda, K.; Gurioli, M. Ultra-narrow emission from single GaAs self-assembled quantum dots grown by droplet epitaxy. *Nanotechnology* **2009**, *20*, 395601.
47. Mlinar, V.; Bozkurt, M.; Ulloa, J.; Ediger, M.; Bester, G.; Badolato, A.; Koenraad, P.; Warburton, R.; Zunger, A. Structure of quantum dots as seen by excitonic spectroscopy versus structural characterization: Using theory to close the loop. *Physical Review B* **2009**, *80*, 165425.
48. Luo, J.W.; Zunger, A. Geometry of epitaxial GaAs/(Al, Ga) As quantum dots as seen by excitonic spectroscopy. *Physical Review B* **2011**, *84*, 235317.
49. Mano, T.; Koguchi, N. Nanometer-scale GaAs ring structure grown by droplet epitaxy. *Journal of crystal growth* **2005**, *278*, 108–112.
50. Mano, T.; Kuroda, T.; Sanguinetti, S.; Ochiai, T.; Tateno, T.; Kim, J.; Noda, T.; Kawabe, M.; Sakoda, K.; Kido, G.; others. Self-assembly of concentric quantum double rings. *Nano letters* **2005**, *5*, 425–428.
51. Somaschini, C.; Bietti, S.; Koguchi, N.; Sanguinetti, S. Fabrication of multiple concentric nanoring structures. *Nano letters* **2009**, *9*, 3419–3424.
52. Shwartz, N.L.; Vasilenko, M.A.; Nastovjak, A.G.; Neizvestny, I.G. Concentric GaAs nanorings formation by droplet epitaxy—Monte Carlo simulation. *Computational Materials Science* **2018**, *141*, 91–100.
53. Sanguinetti, S.; Mano, T.; Kuroda, T. Self-assembled semiconductor quantum ring complexes by droplet epitaxy: growth and physical properties. In *Physics of Quantum Rings*; Springer, 2018; pp. 187–228.
54. Heyn, C.; Zocher, M.; Hansen, W. Functionalization of Droplet Etching for Quantum Rings. In *Physics of Quantum Rings*; Springer, 2018; pp. 139–162.
55. Abbarchi, M.; Mastrandrea, C.; Kuroda, T.; Mano, T.; Sakoda, K.; Koguchi, N.; Sanguinetti, S.; Vinattieri, A.; Gurioli, M. Exciton fine structure in strain-free GaAs/Al 0.3 Ga 0.7 As quantum dots: Extrinsic effects. *Physical Review B* **2008**, *78*, 125321.
56. Plumhof, J.; Křápek, V.; Wang, L.; Schliwa, A.; Bimberg, D.; Rastelli, A.; Schmidt, O. Experimental investigation and modeling of the fine structure splitting of neutral excitons in strain-free GaAs/Al x Ga 1-x As quantum dots. *Physical Review B* **2010**, *81*, 121309.

57. Tong, H.; Wu, M. Theory of excitons in cubic III-V semiconductor GaAs, InAs and GaN quantum dots: fine structure and spin relaxation. *Physical Review B* **2011**, *83*, 235323.
58. Trotta, R.; Zallo, E.; Ortix, C.; Atkinson, P.; Plumhof, J.; Van den Brink, J.; Rastelli, A.; Schmidt, O. Universal recovery of the energy-level degeneracy of bright excitons in InGaAs quantum dots without a structure symmetry. *Physical review letters* **2012**, *109*, 147401.
59. Mahalingam, K.; Otsuka, N.; Melloch, M.; Woodall, J. Arsenic precipitates in Al0. 3Ga0. 7As/GaAs multiple superlattice and quantum well structures. *Applied Physics Letters* **1992**, *60*, 3253–3255.
60. Abbarchi, M.; Mastrandrea, C.; Kuroda, T.; Mano, T.; Vinattieri, A.; Sakoda, K.; Gurioli, M. Poissonian statistics of excitonic complexes in quantum dots. *Journal of Applied Physics* **2009**, *106*, 053504.
61. Kuroda, T.; Belhadj, T.; Abbarchi, M.; Mastrandrea, C.; Gurioli, M.; Mano, T.; Ikeda, N.; Sugimoto, Y.; Asakawa, K.; Koguchi, N.; others. Bunching visibility for correlated photons from single GaAs quantum dots. *Physical Review B* **2009**, *79*, 035330.
62. Accanto, N.; Minari, S.; Cavigli, L.; Bietti, S.; Isella, G.; Vinattieri, A.; Sanguinetti, S.; Gurioli, M. Kinetics of multiexciton complex in gaas quantum dots on si. *Applied Physics Letters* **2013**, *102*, 053109.
63. Abbarchi, M.; Troiani, F.; Mastrandrea, C.; Goldoni, G.; Kuroda, T.; Mano, T.; Sakoda, K.; Koguchi, N.; Sanguinetti, S.; Vinattieri, A.; others. Spectral diffusion and line broadening in single self-assembled Ga As/ Al Ga As quantum dot photoluminescence. *Applied physics letters* **2008**, *93*, 162101.
64. Bester, G.; Zunger, A. Compositional and size-dependent spectroscopic shifts in charged self-assembled In x Ga 1- x A s/G a A s quantum dots. *Physical Review B* **2003**, *68*, 073309.
65. Narvaez, G.A.; Bester, G.; Zunger, A. Excitons, biexcitons, and trions in self-assembled (In, Ga) As/ Ga As quantum dots: Recombination energies, polarization, and radiative lifetimes versus dot height. *Physical Review B* **2005**, *72*, 245318.
66. Schliwa, A.; Winkelnkemper, M.; Bimberg, D. Few-particle energies versus geometry and composition of In x Ga 1- x As/GaAs self-organized quantum dots. *Physical Review B* **2009**, *79*, 075443.
67. Lelong, P.; Bastard, G. Binding energies of excitons and charged excitons in GaAsGa (In) As quantum dots. *Solid state communications* **1996**, *98*, 819–823.
68. Tsuchiya, T.; Katayama, S. A quantum Monte Carlo study on excitonic molecules in quantum wells. *Solid-State Electronics* **1998**, *42*, 1523–1526.
69. Tsuchiya, T. Biexcitons and charged excitons in quantum dots: A quantum Monte Carlo study. *Physica E: Low-Dimensional Systems and Nanostructures* **2000**, *7*, 470–474.
70. Tsuchiya, T. Diffusion Monte Carlo study on biexcitons and charged excitons in semiconductor quantum structures. *Progress of Theoretical Physics Supplement* **2000**, *138*, 128–129.
71. Plumhof, J.D.; Trotta, R.; Rastelli, A.; Schmidt, O.G. Experimental methods of post-growth tuning of the excitonic fine structure splitting in semiconductor quantum dots. *Nanoscale research letters* **2012**, *7*, 1–11.
72. Ferreira, R. Exchange coupling and polarization relaxation in self-assembled quantum dots. *Physica E: Low-dimensional Systems and Nanostructures* **2002**, *13*, 216–219.
73. Seguin, R.; Schliwa, A.; Rodt, S.; Pötschke, K.; Pohl, U.; Bimberg, D. Size-dependent fine-structure splitting in self-organized InAs/GaAs quantum dots. *Physical review letters* **2005**, *95*, 257402.
74. Gong, M.; Hofer, B.; Zallo, E.; Trotta, R.; Luo, J.W.; Schmidt, O.; Zhang, C. Statistical properties of exciton fine structure splitting and polarization angles in quantum dot ensembles. *Physical Review B* **2014**, *89*, 205312.
75. Schimpf, C.; Reindl, M.; Basset, F.B.; Jöns, K.D.; Trotta, R.; Rastelli, A. Quantum dots as potential sources of strongly entangled photons for quantum networks. *arXiv preprint arXiv:2011.12727* **2020**.
76. Abbarchi, M.; Kuroda, T.; Mastrandrea, C.; Vinattieri, A.; Sanguinetti, S.; Mano, T.; Sakoda, K.; Gurioli, M. Fine structure splitting of quantum dot excitons: Role of geometry and environment. *Physica E: Low-dimensional Systems and Nanostructures* **2010**, *42*, 881–883.
77. Belhadj, T.; Amand, T.; Kunold, A.; Simon, C.M.; Kuroda, T.; Abbarchi, M.; Mano, T.; Sakoda, K.; Kunz, S.; Marie, X.; others. Impact of heavy hole-light hole coupling on optical selection rules in GaAs quantum dots. *Applied Physics Letters* **2010**, *97*, 051111.
78. Lin, C.H.; You, W.T.; Chou, H.Y.; Cheng, S.J.; Lin, S.D.; Chang, W.H. Anticorrelation between the splitting and polarization of the exciton fine structure in single self-assembled InAs/GaAs quantum dots. *Physical Review B* **2011**, *83*, 075317.

79. Tonin, C.; Hostein, R.; Voliotis, V.; Grousson, R.; Lemaitre, A.; Martinez, A. Polarization properties of excitonic qubits in single self-assembled quantum dots. *Physical Review B* **2012**, *85*, 155303.
80. Liao, Y.H.; Liao, C.C.; Ku, C.H.; Chang, Y.C.; Cheng, S.J.; Jo, M.; Kuroda, T.; Mano, T.; Abbarchi, M.; Sakoda, K. Geometrical impact on the optical polarization of droplet epitaxial quantum dots. *Physical Review B* **2012**, *86*, 115323.
81. Plumhof, J.; Trotta, R.; Křápek, V.; Zallo, E.; Atkinson, P.; Kumar, S.; Rastelli, A.; Schmidt, O.G. Tuning of the valence band mixing of excitons confined in GaAs/AlGaAs quantum dots via piezoelectric-induced anisotropic strain. *Physical Review B* **2013**, *87*, 075311.
82. Fras, F.; Bernardot, F.; Eble, B.; Bernard, M.; Siarry, B.; Miard, A.; Lemaitre, A.; Testelin, C.; Chamarro, M. The role of heavy–light-hole mixing on the optical initialization of hole spin in InAs quantum dots. *Journal of Physics: Condensed Matter* **2013**, *25*, 202202.
83. Luo, J.W.; Bester, G.; Zunger, A. Supercoupling between heavy-hole and light-hole states in nanostructures. *Physical Review B* **2015**, *92*, 165301.
84. Yuan, X.; Weyhausen-Brinkmann, F.; Martín-Sánchez, J.; Piredda, G.; Křápek, V.; Huo, Y.; Huang, H.; Schimpf, C.; Schmidt, O.G.; Edlinger, J.; others. Uniaxial stress flips the natural quantization axis of a m photonics. *Nature communications* **2018**, *9*, 1–8.